

Enhancing Foundation VLM Robustness to Missing Modality: Scalable Diffusion for Bi-directional Feature Restoration

Wei Dai¹ Haoyu Wang¹ Honghao Chang² Lijun He² Fan Li² Jian Sun³ Haixia Bi²

Abstract

Vision Language Models (VLMs) typically assume complete modality input during inference. However, their effectiveness drops sharply when certain modalities are unavailable or incomplete. Current research primarily faces two dilemmas: Prompt-based methods struggle to restore missing yet indispensable features and impair generalization of VLMs. Imputation-based approaches, lacking effective guidance, are prone to generating semantically irrelevant noise. Restoring precise semantics while sustaining VLM generalization remains challenging. Therefore, we propose a general missing modality restoration strategy in this paper. We introduce an enhanced diffusion model as a pluggable mid-stage training module to effectively restore missing features. Our strategy introduces two key innovations: (I) Dynamic Modality Gating, which adaptively leverages conditional features to steer the generation of semantically consistent features; (II) Cross-Modal Mutual Learning mechanism, which bridges the semantic spaces of dual encoders to achieve bidirectional alignment. Zero-shot evaluations across benchmark datasets demonstrate that our approach outperforms existing baseline methods. Extensive experiments and ablation studies confirm our model as a robust and scalable extension for VLMs in missing modality scenarios, ensuring reliability across diverse missing rates and environments. Our code and models will be publicly available.

1. Introduction

Multimodal learning has achieved remarkable success in the fields of vision and language. In particular, foundational Vision Language Models (VLMs) represented by

¹Xi'an Jiaotong University ²School of Information and Communications Engineering, Xi'an Jiaotong University ³School of Mathematics and Statistics, Xi'an Jiaotong University.

Correspondence to: Haixia Bi <haixia.bi@xjtu.edu.cn>.

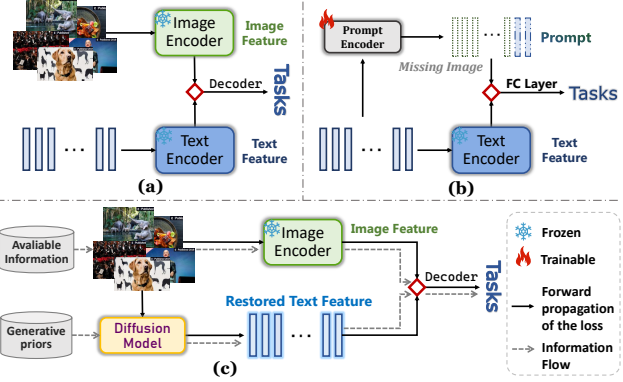


Figure 1. An overview of Multimodal Missing Modalities: (a) Foundation VLM working with complete modality; (b) Prompt learning methods for missing modalities; (c) (Ours) Feature restoration method for missing modalities utilizing Diffusion model.

CLIP (Radford et al., 2021) and BLIP (Li et al., 2022) have constructed a cross-modal semantic space through large-scale contrastive pretraining. However, these models are typically built on the idealized assumption that all modalities are fully available during the inference phase. In real-world deployment, missing modality has become a critical bottleneck constraining the practical performance of VLMs due to factors such as collection costs and privacy protection.

Existing research on missing modalities primarily falls into two categories: Prompt-based methods (Shi et al., 2024; Zhang et al., 2025; Zhao et al., 2025) adapt to missing modalities via learnable prompts, but often compromise the VLM generalization by introducing task-specific parameters and altering the model's original architectures. As a result, these methods provide only dataset-dependent adaptations rather than true feature restoration, limiting their utility in tasks requiring complete features. Imputation-based methods (Ma et al., 2021; Xu et al., 2025) attempt to reconstruct the missing modalities. But prior generative models are prone to producing semantically irrelevant noise in the absence of strong guidance. A core challenge lies in restoring missing features accurately while maintaining consistency with existing modalities on the deep semantic manifold.

To overcome these limitations, this paper proposes a feature restoration strategy based on a Scalable Diffusion Model.

Unlike conventional strategies that rely on shallow MLP-based projections or static constant padding (e.g., filling missing entries with zeros), the diffusion model exploits its robust generative priors to capture the intricate manifold geometry inherent in the VLM’s semantic space (Figure 1). Through step-by-step denoising, the model can completely restore missing VLM features, making it applicable across various tasks and scenarios, thereby genuinely enhancing the robustness and generalization of VLMs under incomplete inputs. By performing mid-stage training within the VLM feature space, we transform the generative prior of the diffusion model into semantic information increment. This increment not only compensates for the lost original semantics but also serves as a powerful information augmentation, effectively bridging the semantic gap between unimodal inputs and multimodal representations.

To enable the diffusion model to accurately extract key semantic information while suppressing modality-irrelevant noise, we propose **Dynamic Modality Gating** mechanism. This mechanism leverages conditional features from available modalities to keep task-relevant information and filter out noise. By utilizing diffusion priors, it enhances the signal-to-noise ratio and maintains semantic consistency throughout the generative process. To achieve high-quality bidirectional feature restoration under conditions of missing modalities, we propose **Cross-modal Mutual Learning** mechanism. This mechanism bridges the latent semantic spaces of visual and text encoders to achieve alignment across bidirectional semantic manifolds. It prevents the synthesized features from deviating from the target semantic space, addresses the uncertainty inherent in unidirectional mapping, and reinforces the robustness of both Image-to-Text (I2T) and Text-to-Image (T2I) restoration.

We conducted zero-shot generalization experiments on four benchmark datasets, and the results demonstrate that our restorative mid-stage-trained model outperforms existing strong baselines in missing modality tasks. This indicates its capability to successfully restore semantically consistent features on unseen datasets, significantly boosting downstream task performance. Our contributions are as follows:

- We propose a scalable framework based on diffusion models that moves beyond simplistic feature imputation to achieve high-fidelity semantic restoration within VLM latent spaces.
- We introduce the Dynamic Modality Gating and Cross-modal Mutual Learning mechanisms, which effectively filter modality noise and enforce bidirectional semantic alignment through cyclic consistency.
- Through mid-stage training on large datasets, we demonstrate that our approach greatly enhances VLM robustness in incomplete modality scenarios, establishing a new benchmark for building universal missing-robust models.

2. Related Work

2.1. Multimodal Learning with Missing Modalities

The problem of missing modalities (Zhao et al., 2021; Khat-tak et al., 2023; Ma et al., 2022; Wang et al., 2023) has emerged as a significant research field. Existing methods can be categorized into the following two types:

Prompt-based Methods aim to adapt foundation models to incomplete inputs by introducing a limited number of learnable prompts (Jang et al., 2024). Notable examples include modality-missing-aware prompts (Lee et al., 2023), modality-specific prompts (Jia et al., 2022), Deep Correlated Prompting (Shi et al., 2024), Synergistic Prompt (Zhang et al., 2025), and Memory-Driven Prompts (Zhao et al., 2025). Furthermore, PROMISE (Chen et al., 2025) developed prompt-attention with modality-specific prompt pools. Reflecting the earlier statement, the lack of robust generalizability remains a major drawback of prompt-based methods.

Generation and Imputation Methods attempt to explicitly reconstruct missing information. Early research, such as SMIL (Ma et al., 2021), utilizes Bayesian Meta-learning to handle missing data. Missing Modality Prediction (Kim & Kim, 2024) employs trainable prompts to predict missing features, while McMoE (Xu et al., 2025) utilizes an adaptive gated modality generator network to synthesize missing characteristics. In particular, Retrieval-augmented Methods leverage external knowledge. RAGPT (Lang et al., 2025a) framework identifies similar instances through a retriever, and REDEEM (Lang et al., 2025b) further introduces retrieval-guided generation utilizing a memory bank. However, previous generation and imputation strategies often face a trade-off between sub-optimal performance and high memory consumption (e.g., memory banks).

2.2. Diffusion Models for Semantic Latent Modeling

Diffusion Models (Sohl-Dickstein et al., 2015; Peebles & Xie, 2023) have demonstrated great potential in image synthesis (Dhariwal & Nichol, 2021; Rombach et al., 2022), video generation (Ho et al., 2022), and various discriminative tasks (Li et al., 2023), owing to their superior distribution modeling capabilities. Diffusion models gradually transform data into Gaussian noise via a forward diffusion process, subsequently learning a reverse denoising process to recover the original data distribution from the noise (Ho et al., 2020). Compared to GANs (Goodfellow et al., 2014) and VAEs (Kingma & Welling, 2013), diffusion models can better capture the complex structures of high-dimensional manifolds, avoiding training instability and model collapse.

Prior research (Ramesh et al., 2022; Becker et al., 2025) provide oblique evidence that the latent representations generated by diffusion models exhibit high semantic consistency. For instance, advanced diffusion variants have been

employed for feature-level augmentation, generating high-quality synthetic features (Chen et al., 2023; Amit et al., 2021). In this work, we leverage the powerful generative priors of diffusion models in the feature space, designing them as a pluggable mid-stage training module. Through the two mechanisms, our approach precisely restores the semantic information of missing modalities, significantly enhancing the robustness of foundation Vision Language Models while maintaining their inherent generalizability.

3. Our Method

3.1. Preliminaries

Problem Definition This paper investigates the missing modality scenario in multimodal learning. Without loss of generality, we study the input case involving $M = 2$ modalities, denoted as m_1 and m_2 (e.g., text and image). This setting can be naturally extended to more complex multimodal scenarios. Specifically, the multimodal dataset during the inference stage can be represented as: $D = \{D_c, D_{m_1}, D_{m_2}\}$ where the subsets are defined as follows: The complete-modality subset $D_c = \{(x_{m_1}, x_{m_2}, y)\}$ includes inputs x from all modalities and their corresponding labels y . The missing-modality subsets: $D_{m_1} = \{(x_{m_1}, y)\}$, $D_{m_2} = \{(x_{m_2}, y)\}$ represent the scenarios where one of the modalities is missing (e.g., missing text or missing image).

Our Framework To address missing modalities, the framework first leverages a pretrained foundational VLM to extract latent features from the available modality: $z_{m_1} = \text{Encoder}(x_{m_1})$. Conditioned on z_{m_1} , the missing feature is explicitly restored via an iterative DDIM process. Starting from Gaussian noise $z_T \sim \mathcal{N}(0, \mathbf{I})$ with dimensions matching the latent space, the feature \hat{z}_{m_2} is reconstructed through the following deterministic transition:

$$z_{t-1} = \sqrt{\bar{\alpha}_{t-1}} \left(\frac{z_t - \sqrt{1 - \bar{\alpha}_t} \epsilon_\theta(z_t, t | z_{m_1})}{\sqrt{\bar{\alpha}_t}} \right) + \sqrt{1 - \bar{\alpha}_{t-1}} \epsilon_\theta(z_t, t | z_{m_1}) \quad (1)$$

where the final restored feature $\hat{z}_{m_2} = z_0$ is obtained after T inference steps. Subsequently, the available and restored features are concatenated and processed by a lightweight decoder for the classification task: $y = \text{Decoder}([z_{m_1}; \hat{z}_{m_2}])$.

3.2. Dynamic Modality Gating

In the context of missing modality generation, the conventional structure of attention mechanisms and FFN in deep Transformers magnify several limitations: **Low Feature-Background Discrimination:** Standard attention often fails to decouple critical semantic features from irrelevant background noise, which becomes particularly important when one modality is absent and the model must rely on limited

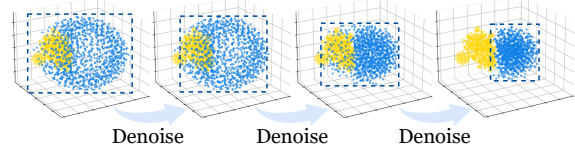


Figure 2. PCA visualization of 1,000 samples shows that our model aligns the restored features with ground-truth (from left to right $T = 1000, 800, 500, 50$) via the denoising sampling process.

information. **Information Dilution:** In long-sequence processing, attention weights are distributed over numerous tokens, weakening the representation intensity of key information. **Lack of Adaptive Control:** There is no inherent mechanism to dynamically modulate the focus and intensity of modality interactions.

To overcome these limitations, we integrate a modality gating unit into the Diffusion Transformer block (containing a self-attention layer, a cross-attention layer and a FFN) to dynamically guide the feature restoration process. We replace the direct connection with a dynamic gating mechanism conditioned on global semantics and the diffusion timestep. Specifically, we first fuse the timestep embedding t_{emb} into the condition C : $C = \text{Condition}_{emb} + \text{MLP}_{time}(t_{emb})$. Subsequently, an attention pooling is utilized, where query probes (serving as learnable embedding weights) aggregate key semantics from the fused features:

$$G_{pooled} = \text{Softmax} \left(\frac{Q_{probe}(W_K C)^T}{\sqrt{d_k}} \right) (W_V C) \quad (2)$$

A non-linear mapping then produces the channel-wise modulation vector G :

$$G = \text{MLP}_{gate}(G_{pooled}) \quad (3)$$

Within each Transformer block, specialized activation coefficients for the self-attention and MLP layers are computed via linear projection and Sigmoid activation:

$$Z_{attn} = \sigma(W_{attn}G + b_{attn}), \quad Z_{mlp} = \sigma(W_{mlp}G + b_{mlp}) \quad (4)$$

The gating unit adaptively regulates the information flow across feature channels using these weights:

$$x_{mid} = x + Z_{attn} \odot \text{Self-Attention}(\text{LN}(x)) \quad (5)$$

$$x_{out} = x_{mid} + Z_{mlp} \odot \text{MLP}(\text{LN}(x_{mid})) \quad (6)$$

where \odot denotes the element-wise product.

This learnable gating mechanism acts as a secondary filter, enhancing the signal-to-noise ratio of critical features. By suppressing irrelevant information flow, it effectively preserves the most salient cross-modal representations, providing robust guidance for generation.

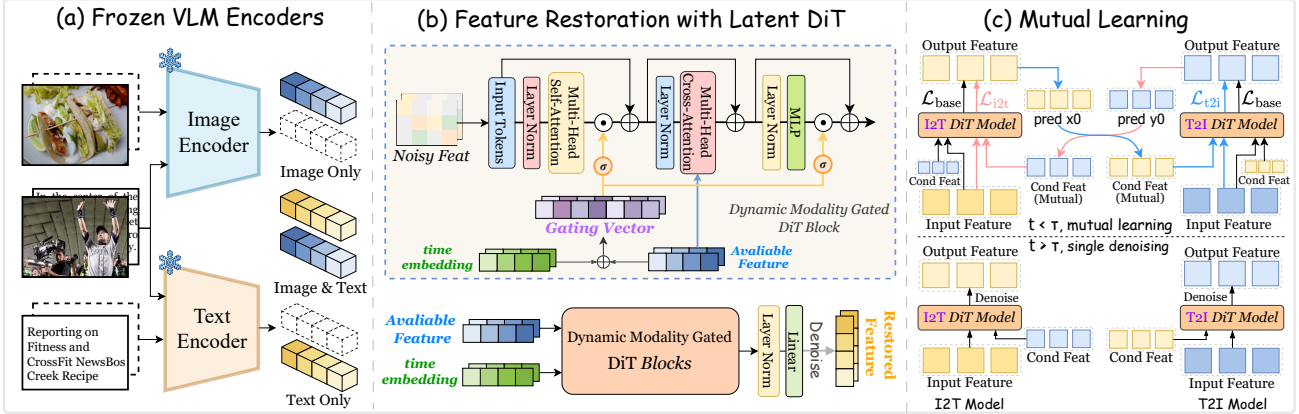


Figure 3. The architecture of our Missing Modality Restoration Framework. (a) Feature extraction process for available modalities utilizing frozen pre-trained VLM Encoders. (b) The top section depicts the gating mechanism of the DiT backbone, and the bottom section provides a conceptual illustration of how the diffusion model reshapes the feature distribution. (c) Architectural design of the mutual learning mechanism, incorporating multi-objective loss functions within specific denoising intervals.

3.3. Mutual Learning Mechanism

We introduce a diffusion-based Mutual Learning framework that replaces isolated modality mappings with a bidirectional closed-loop system. By explicitly aligning I2T and T2I directions, our method prevents semantic drift and improves reconstruction quality under high cross-modal uncertainty.

In the first stage of training, the model learns uni-directional mappings by minimizing the noise estimation error. For a given clean feature x_0 and conditional feature c , at a random timestep $t \sim [0, T]$, a noisy sample x_t is generated through the forward diffusion process. The base training loss L_{base} is defined as the mean squared error between the predicted noise and the ground-truth Gaussian noise ϵ :

$$L_{base} = \mathbb{E}_{x_0, \epsilon, t} [\|\epsilon - \epsilon_\theta(x_t, c, t)\|^2] \quad (7)$$

To realize the “predict-and-reconstruct” closed loop, we perform a second stage of training. When the diffusion timestep t is below a preset threshold τ (set to 50 in our experiments), the system is in a critical stage of denoising, where the quality of features generated by the model is vital for semantic alignment. First, the estimated value of the clean feature \hat{x}_0 is derived from the noisy sample x_t using the noise ϵ_θ predicted by the model:

$$\hat{x}_0 = \frac{1}{\sqrt{\alpha_t}} x_t - \sqrt{\frac{1}{\alpha_t} - 1} \epsilon_\theta(x_t, c, t) \quad (8)$$

The mutual learning consistency loss L_{mutual} requires that the restored feature estimate \hat{x}_0 serves as an effective condition to guide the reverse-mapping model. For instance, the restored image feature $\hat{x}_{0, img}$ must be able to assist the text diffusion model in accurately predicting the text modality noise ϵ_{txt} . The bi-directional mutual learning consistency

loss function is defined as:

$$L_{mutual} = \mathbb{E} \left[\|\epsilon_{txt} - \epsilon_{\theta, i2t}(x_{t, txt}, \hat{x}_{0, img}, t)\|^2 + \|\epsilon_{img} - \epsilon_{\theta, t2i}(x_{t, img}, \hat{x}_{0, txt}, t)\|^2 \right] \quad (9)$$

where the former term characterizes the I2T consistency loss that evaluates the conditional accuracy of restored image features and the latter term represents the T2I consistency loss. In this way, the restored features are forced to be in the intelligible space of the other modality.

It is worth noting that we found that if L_{mutual} is used as the sole loss, the model tends to learn an identity mapping, neglecting the reconstruction accuracy of the original latent features. The final loss function L_{total} integrates the mutual learning loss and the base mapping regularization loss:

$$L_{total} = L_{mutual} + L_{base, i2t} + L_{base, t2i} \quad (10)$$

Through joint training, the I2T and T2I models serve as mutual regularizers for each other. This explicit alignment mechanism effectively solves the problem of cross-modal semantic misalignment in uni-directional diffusion.

3.4. Restorative Mid-Stage Training

To further bolster the model’s resilience against missing modalities, we introduce a restorative mid-stage training stage after VLM’s standard contrastive alignment. By leveraging an enhanced DiT-based diffusion backbone, our framework benefits from superior scalability, enabling adaptation to diverse data scales and task requirements. Training is conducted on high-quality, large-scale benchmarks like CC3M and COCO. This strategic choice ensures the acquisition of robust, generalizable semantic embeddings that effectively span the comprehensive latent manifold established by VLM. Our overview framework is shown in Figure 3.

Table 1. Performance comparisons of our method with various baseline methods on four datasets: Our method achieves state-of-the-art (SOTA) across the board. This experiment uses a Zero-Shot mode of our 20-layer diffusion model pre-trained on the CC3M dataset.

Dataset	MM-IMDb			N24News			MMHS11K			Food101		
	Image	Text	Both									
Missing Type	F1-M	F1-M	F1-M	ACC								
Method	F1-M	F1-M	F1-M	ACC								
MAP (CVPR'23)	38.74	47.44	39.13	61.34	57.67	57.78	78.28	72.59	75.73	86.72	74.16	78.42
RAGPT (AAAI'25)	38.82	54.33	49.55	61.18	57.14	60.81	76.93	73.18	74.94	82.42	76.51	77.54
REDEEM (KDD'25)	47.20	56.32	50.52	63.90	59.17	61.40	78.31	71.66	74.67	83.78	77.52	78.77
MDP (IJCAI'25)	48.61	40.36	41.62	62.13	58.29	59.20	54.36	74.22	54.12	87.07	75.00	79.62
DCP (NeurIPS'24)	51.15	47.58	47.47	67.82	57.83	61.82	71.66	73.64	70.38	87.74	77.82	81.83
SyP (ICCV'25)	50.16	46.52	48.02	67.73	57.64	61.73	70.73	73.87	70.85	87.82	78.01	81.27
Ours	58.22	57.24	57.49	71.70	61.89	65.97	86.47	79.55	82.00	88.37	78.71	83.01
Improve (%)	+7.07	+0.92	+6.97	+3.88	+2.72	+4.15	+8.16	+5.33	+6.27	+0.55	+0.70	+1.18

4. Experiments

4.1. Datasets and Evaluation Metrics

Datasets Following prior research, we evaluated our method on four representative downstream tasks: (1) *MM-IMDb* (Arevalo et al., 2017): Primarily used for multi-label movie genre classification, involving both image and text modalities. (2) *N24News* (Wang et al., 2022): Designed for multi-modal news classification, integrating news images and text across 24 categories. (3) *MMHS11K* (Saddozai et al., 2025): Focused on multi-modal hate speech detection, containing images paired with their corresponding text. (4) *Food101* (Bossard et al., 2014): Focused on food classification through the fusion of images and text. All dataset splits were kept consistent with the original publications.

Baseline Methods We compare our method against six highly competitive baselines, ranging from prompt-based methods to cross-modal retrieval-generation approaches. Specifically, these include: Missing-Aware Prompting (Lee et al., 2023), RAGPT (Lang et al., 2025a), REDEEM (Lang et al., 2025b), Memory-Driven Prompting (Zhao et al., 2025), Deep Correlated Prompting (Shi et al., 2024), and Synergistic Prompting (Zhang et al., 2025).

Evaluation Metrics Following established protocols in prior literature, we employ task-specific evaluation metrics for each dataset: F1-Macro (F1-M) is utilized for the *MM-IMDb* dataset, while Accuracy (ACC) is adopted for the *Food101*, *N24News* and *MMHS11K* datasets.

Missing Pattern Settings The missing rate $\eta\%$ is defined as the fraction of incomplete samples within the total dataset. Specifically, we investigate three distinct missing modality configurations: Single Modality Missing (Text or Image): Given a missing rate $\eta\%$, a subset of $\eta\%$ of the total samples is restricted to a single modality (either text-only or image-

only), while the remaining $(1 - \eta)\%$ consists of complete multimodal pairs. Both Modalities Missing: In this scenario, the missing modalities are distributed equally across both domains. Specifically, $\frac{\eta}{2}\%$ of the dataset consists of image-only samples, $\frac{\eta}{2}\%$ contains only text, and the remaining $(1 - \eta)\%$ of the data remains complete with both modalities.

4.2. Implementation Details

Following prior research, we employ a pre-trained CLIP as the frozen VLM network and utilize several large-scale multimodal datasets as our restorative mid-stage training datasets. Specifically, all our primary experiments adopt CLIP ViT-B/32 as the base VLM and CC3M (Sharma et al., 2018) as the mid-stage training dataset. For downstream tasks, we train an extremely lightweight decoder consisting of a transformer with only two self-attention layers and one cross-attention layer, along with a classifier, meanwhile, the DiT network is frozen and set to evaluation mode only.

For restorative mid-stage training, we use the AdamW optimizer with a learning rate of 1×10^{-4} , accompanied by cosine annealing and linear warm-up. Mixed-Precision (BF16) is employed, and the parameters of the Diffusion network are optimized over a total of 40 epochs. These experiments are conducted on a NVIDIA A800 GPU. For the training of downstream tasks, we use the AdamW optimizer with a learning rate of 5×10^{-4} , which decays by a factor of 0.1 at the midpoint of training. The decoder parameters are optimized for a total of 20 epochs. All experiments and the baseline methods are performed using the same single NVIDIA RTX A5000 GPU (24GB).

For inference, the diffusion model uses DDIM sampling with 50 steps. In Dynamic Modality Gating, we initialize the bias terms of the mapping layers (e.g., -5.0) to make the model prone to improve numerical stability during large-

scale training. In the Mutual Learning Mechanism, we set the coefficient of the threshold to $\tau = 50$. Detailed descriptions regarding the restorative mid-stage training datasets, the number of DiT layers and varying missing rates can be found in the Ablation Study.

4.3. Main Results

To verify the superiority of our mid-stage training feature restoration method, we compare the **Zero-shot** generalization of our Diffusion module against six highly competitive baseline models across four datasets with a missing rate $\eta\% = 70\%$. From results in Table 1, we derive the following observations. Under various modality conditions and metrics, our method consistently outperforms all strong baselines across the four datasets. Specifically, on the *MM-IMDb* dataset (missing image), the F1-M metric improved by 7.07%, and on the *MMHS11K* dataset (missing image), the ACC improved by 8.16%. Notably, during downstream task testing, our method completely freezes the pre-trained Diffusion module and only trains task-specific decoders for classification. Our Diffusion module is capable of restoring features even without having seen the downstream datasets, achieving state-of-the-art (SOTA) performance. These results validate that our restoration pre-trained module can perform zero-shot generalization to restore high-quality modal features, thereby enhancing the model’s robustness in modality-missing scenarios while maintaining the generalization capabilities of the pre-trained VLM.

Conversely, generation methods based on imputation and retrieval show suboptimal performance. This is primarily due to the noise introduced by heuristic data padding and the inherent semantic gap during the retrieval process. These factors, coupled with the challenges of modality heterogeneity during reconstruction, create significant performance bottlenecks. Furthermore, prompt-based methods exhibit limited effectiveness in missing-modality scenarios; their reliance on virtual imputation and static prompting strategies restricts their adaptability, ultimately leading to performance stagnation. Additionally, prompt-based methods may impose constraints on application scenarios, as they cannot be applied to tasks that require complete features for decoding.

4.4. Ablation Study

Ablation of Dynamic Modality Gating To analyze the impact of Dynamic Modality Gating in our improved Diffusion Transformer, we select two variants originally proposed in Diffusion models and widely applied in image generation tasks, along with a baseline: (1) Adaptive LayerNorm (AdaLN): Utilizing AdaLN instead of our gating mechanism to achieve linear scaling of features; (2) Concat: Simply concatenating conditional features with original features and appending an MLP to scale the feature dimensions; (3)

Table 2. Ablation Study of different modules on *MMHS11K* and *N24News* (under 70% missing modality and 20 DiT modules).

Method	MMHS11K			N24News		
	Image	Text	Both	Image	Text	Both
Ours (All)	86.47	79.55	82.00	71.70	61.89	65.97
Mutual	<u>85.27</u>	<u>76.94</u>	<u>80.79</u>	<u>71.37</u>	<u>61.38</u>	<u>65.15</u>
Base	84.06	76.23	80.11	70.18	60.05	63.37
Gating	<u>85.64</u>	<u>78.00</u>	<u>80.77</u>	<u>71.38</u>	<u>61.48</u>	<u>64.93</u>
AdaLN	84.44	77.33	80.64	70.77	60.50	63.88
Concat	80.05	72.14	76.44	65.21	54.95	59.63
Base	84.06	76.23	80.11	70.18	60.05	63.37

Baseline (No improvement): Completely removing the gating mechanism while retaining only the basic framework. As shown in Table 2, our ablation study demonstrate that the Modality Gating mechanism achieves the superior performance. We attribute its effectiveness to its ability to filter components containing critical semantic information while simultaneously suppressing modality-irrelevant noise in missing-modality tasks, thereby achieving precise control over the output. In contrast, other methods suffer from a “pass-through” nature, where irrelevant information cannot be effectively filtered, ultimately weakening the utility of the resulting features.

Ablation of Mutual Learning Mechanism To evaluate the impact of the Mutual Learning Mechanism on the Diffusion model, we designed the following experiments: (1) With Mutual Learning Mechanism: Applying Mutual Learning with a threshold of $\tau = 50$ through a two-stage training process (40 Epochs and 20 Epochs);(2) Without Mutual Learning : Completely removing the Mutual Learning Mechanism and conducting only a single-stage training. We observe that the Mutual Learning Mechanism improves performance. This finding supports our assertion that the Mutual Learning Mechanism effectively addresses the issue of semantic drift in unidirectional diffusion, ensuring that the features generated by the model possess bidirectional interchangeability beneficial for downstream tasks.

Effect of Dynamic Modality Gating To further investigate the essence of our Gating and explore whether the model can automatically prune meaningless components of the output, we perform a visualization analysis of the gates, as illustrated in Figure 4. The visualization results reveal distinct sparsity in the gates following the attention, proving that the gating mechanism effectively functions as a filter. Observations of the gates following the MLP indicate that the overall activation intensity gradually decreases as the

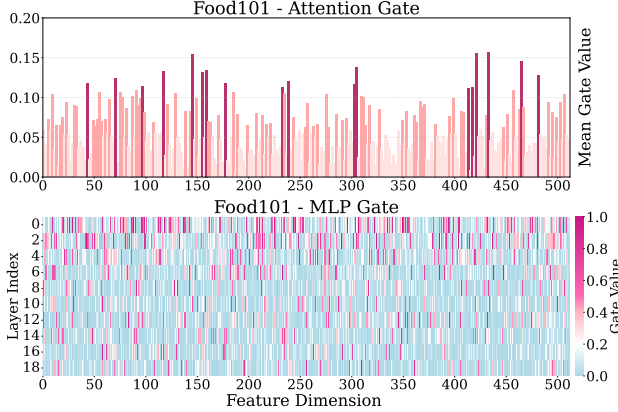


Figure 4. The visualization of Dynamic Modality Gating: The top plot shows the average activation values of each channel after attention-based gating. The bottom plot shows the activation values of each channel at different DiT depths.

depth of the network increases. This suggests that in shallower DiT modules, the model needs to incorporate more information from conditional features, thereby requiring more channels to preserve initialization information. Conversely, in deeper DiT modules, the model prioritizes the selection of critical semantic information while subtracting more irrelevant noise, resulting in a lower overall activation intensity across most channels. During the training process, we observed that the mean value of the gates at the output is approximately 0.1, with the vast majority of values falling within the range 0 – 0.2. The model automatically optimizes the gates to become zero-valued for most entries while magnifying only the essential features. Overall, our modality gating evolves into a sparse “selector”.

4.5. Model Scalability

Restorative Mid-Stage Training Datasets To verify the scalability of our model, we conducted mid-stage training of the diffusion model on image-text pair datasets of varying scales and evaluated its performance across multiple downstream tasks. The experimental results Table 3 demonstrate that our method possesses exceptional versatility and scalability. First, when trained on small-scale datasets (e.g., *Food101* (Bossard et al., 2014)), the model still achieves highly competitive performance on tasks such as *MM-IMDb* and *N24News*. This proves that the DiT-based diffusion architecture can efficiently capture the underlying semantic priors of the CLIP manifold, indicating a robust capability for feature restoration even with limited data. Second, as the mid-stage training data scale expands from 0.44M (COCO (Lin et al., 2014)) to 3M (CC3M (Sharma et al., 2018)), all metrics for downstream tasks exhibit a clear increasing trend. For instance, in the image-missing scenario of *MMHS11K*, accuracy improves from 85.14% to 86.47%. The significant performance gains validate the strong scaling potential of the framework, which can effectively leverage

Table 3. Performance comparison with different sizes of mid-stage training datasets (with 70% missing modality and 20 DiT blocks).

Pretraining	Size	MM-IMDb			MMHS11K		
		Image	Text	Both	Image	Text	Both
CC3M (Ours)	3M	58.22	57.24	57.49	86.47	79.55	82.00
COCO+Flickr30k	475K	57.57	57.12	57.19	85.59	78.77	81.23
COCO	445K	57.08	56.90	56.67	85.14	78.68	80.95
Food101	68K	56.60	55.48	55.97	83.66	76.09	78.24
Baseline (DCP)	-	51.15	47.58	47.47	71.66	73.64	70.38

Table 4. Performance comparison with various DiT depths (with 70% missing modality and CC3M dataset).

DiT Depth	MM-IMDb			N24News			MMHS11K		
	Image	Text	Both	Image	Text	Both	Image	Text	Both
Depth = 16	57.37	56.20	57.01	71.16	61.39	65.31	85.79	79.61	81.20
Depth = 18	57.79	56.46	57.20	71.24	61.46	65.33	85.82	79.59	81.27
Depth = 20	58.22	57.24	57.49	71.70	61.89	65.97	86.47	79.55	82.00
Depth = 22	57.38	57.78	56.93	72.01	61.76	65.77	85.55	79.45	81.68
Depth = 24	57.18	56.99	56.42	71.11	61.97	65.71	85.05	78.36	82.41

large-scale, high-quality multimodal data to continuously enhance the robustness of multimodal representations.

Number of DiT Layers To investigate the impact of model scale on the effectiveness of feature restoration, we conducted an ablation study on the depth of the DiT architecture based on CC3M mid-stage training. The experimental results are presented in Table 4. As the model depth increases from 16 to 20 layers, the performance across the three downstream tasks (*MM-IMDb*, *N24News* and *MMHS11K*) under various missing modality scenarios shows a clear improvement. This indicates that appropriately increasing the depth of the Transformer layers significantly enhances the model’s ability to model the complex CLIP manifold space. However, when the depth is further increased to 22 or 24 layers, the performance gains begin to exhibit diminishing marginal returns, with slight fluctuations or declines observed in certain metrics. This is likely attributable to overfitting caused by the excessive number of model parameters. Considering both inference efficiency and classification accuracy, we adopted a 20-layer DiT structure in our final framework, as it represents the optimal balance between model performance and computational overhead.

4.6. Robustness to Different Missing Rates

We conducted an experiment to analyze the robustness of our model against different missing rates. The Figure 5 illustrates the comparative results between our method and four strong baseline models (MAP, MDP, DCP, and SyP)

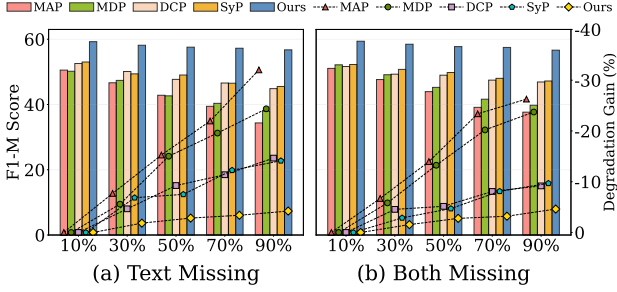


Figure 5. Robustness analysis on the *MM-IMDb* dataset across various missing rates in terms of F1-M.

on the *MM-IMDb* dataset. We observe that the performance of all baseline models degrades significantly as the missing rate increases, with the degree of decline exceeding 10% (across the range of 10% to 90% missing rates). In contrast, the performance of our method only decreases slightly with the increase in missing rate, showing a decline of only approximately 3%. This result highlights that our restorative mid-stage training module, serving as an extension of the base VLM, effectively restores features with consistent semantic information, thereby enhancing effectiveness under extremely high missing rates.

4.7. Visualization of Model Effectiveness

T-SNE Analysis of Reconstructed Features To visually evaluate the semantic fidelity of the restored representations, we conduct a 2D t-SNE visualization of the restored image and text features, as shown in Figure 6. Qualitative analysis reveals that the restored features exhibit robust cluster cohesion and manifold separation within the 2D space. This “denoising” phenomenon confirms that the DiT model effectively filters out modality noise and maps features onto more discriminative semantic centers. The distinct category boundaries in the 2D visualization indicate that, even in the absence of dense visual priors, the model successfully achieves a restoration from individual details toward core categorical semantics.

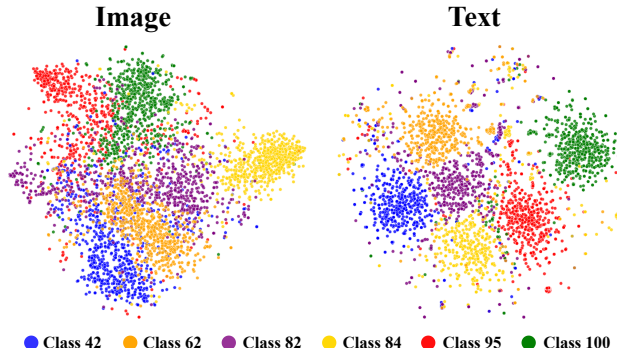


Figure 6. T-SNE analysis of restored features on the *Food101* dataset, where we visualize the two-dimensional multimodal embedding distribution of specific categories.

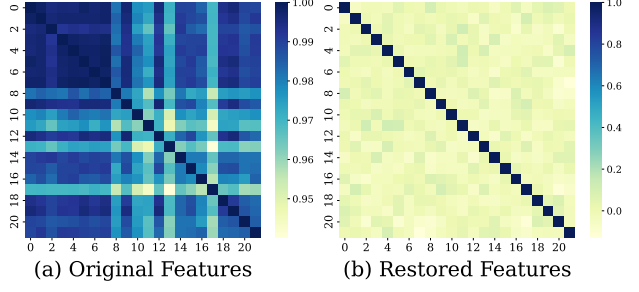


Figure 7. Category-wise cosine similarity for 1,000 features in *MM-IMDb* datasets. The original CLIP features (left) and our restored counterparts (right) exhibit high semantic alignment.

Semantic Fidelity Analysis of Restored Features To evaluate the semantic fidelity of the restored latent representations, we compare the original CLIP visual features f_{real} with the reconstructed features f_{recon} by visualizing inter-class similarity matrices across 19 categories in *MM-IMDb*. As illustrated in Figure 7, the restored similarity matrix exhibits a more pronounced diagonal structure compared to the original CLIP features. While the original features reveal inherent semantic correlations between similar categories, the restored features demonstrate lower inter-class similarity, suggesting that our DiT model effectively maps text-guided semantics into highly discriminative clusters. The clear separation between categories indicates that the diffusion process successfully mitigates modal noise and reinforces class boundary constraints.

4.8. Further Analysis and Discussions

Beyond the primary evaluations, we conduct extensive supplementary analyses to validate our framework’s utility. Specifically, we investigate the impact of sampling steps on inference efficiency and explore the sensitivity of threshold τ . Furthermore, we demonstrate our method’s portability by integrating it with existing frameworks, showing consistent performance gains. Detailed quantitative results, and in-depth discussions could be found in Appendix.

5. Conclusion

This paper proposes a restoration strategy that aims to address the challenges of missing modalities. We leverage an improved Diffusion model to effectively restore missing features, serving as a restorative mid-stage training module that significantly enhances the robustness and generalization of foundational Vision Language Models (VLMs) under modality-incomplete scenarios. The framework comprises two key components: a Dynamic Modality Gating mechanism and a Cross-modal Mutual Learning mechanism. Extensive experiments conducted across four benchmark datasets demonstrate that our model serves as an effective extension of VLMs for handling missing modalities.

Impact Statement

This paper presents work whose goal is to advance the field of machine learning and robotics. There are many potential societal consequences of our work, none of which we feel must be specifically highlighted here.

References

- Amit, T., Shaharbany, T., Nachmani, E., and Wolf, L. Segdiff: Image segmentation with diffusion probabilistic models. *arXiv preprint arXiv:2112.00390*, 2021.
- Arevalo, J., Solorio, T., Montes-y Gómez, M., and González, F. A. Gated multimodal units for information fusion. *arXiv preprint arXiv:1702.01992*, 2017.
- Becker, J., Wendler, C., Baylies, P., West, R., and Wressnegger, C. Controlling latent diffusion using latent clip. *arXiv preprint arXiv:2503.08455*, 2025.
- Bossard, L., Guillaumin, M., and Van Gool, L. Food-101 – mining discriminative components with random forests. In *European Conference on Computer Vision*, 2014.
- Chen, J., Cheng, S., Yuan, Y., Zhang, Y., Yuan, H., Peng, P., and Zhong, Y. Promise: Prompt-attentive hierarchical contrastive learning for robust cross-modal representation with missing modalities. *arXiv preprint arXiv:2511.10997*, 2025.
- Chen, S., Sun, P., Song, Y., and Luo, P. Diffusiondet: Diffusion model for object detection. In *Proceedings of the IEEE/CVF international conference on computer vision*, pp. 19830–19843, 2023.
- Dhariwal, P. and Nichol, A. Diffusion models beat gans on image synthesis. *Advances in neural information processing systems*, 34:8780–8794, 2021.
- Goodfellow, I. J., Pouget-Abadie, J., Mirza, M., Xu, B., Warde-Farley, D., Ozair, S., Courville, A., and Bengio, Y. Generative adversarial nets. *Advances in neural information processing systems*, 27, 2014.
- Ho, J., Jain, A., and Abbeel, P. Denoising diffusion probabilistic models. *Advances in neural information processing systems*, 33:6840–6851, 2020.
- Ho, J., Salimans, T., Gritsenko, A., Chan, W., Norouzi, M., and Fleet, D. J. Video diffusion models. *Advances in neural information processing systems*, 35:8633–8646, 2022.
- Jang, J., Wang, Y., and Kim, C. Towards robust multimodal prompting with missing modalities. In *ICASSP 2024-2024 IEEE International Conference on Acoustics, Speech and Signal Processing (ICASSP)*, pp. 8070–8074. IEEE, 2024.
- Jia, M., Tang, L., Chen, B.-C., Cardie, C., Belongie, S., Hariharan, B., and Lim, S.-N. Visual prompt tuning. In *European conference on computer vision*, pp. 709–727. Springer, 2022.
- Khattak, M. U., Rasheed, H., Maaz, M., Khan, S., and Khan, F. S. Maple: Multi-modal prompt learning. In *Proceedings of the IEEE/CVF conference on computer vision and pattern recognition*, pp. 19113–19122, 2023.
- Kim, D. and Kim, T. Missing modality prediction for unpaired multimodal learning via joint embedding of unimodal models. In *European Conference on Computer Vision*, pp. 171–187. Springer, 2024.
- Kingma, D. P. and Welling, M. Auto-encoding variational bayes. *arXiv preprint arXiv:1312.6114*, 2013.
- Lang, J., Cheng, Z., Zhong, T., and Zhou, F. Retrieval-augmented dynamic prompt tuning for incomplete multimodal learning. In *Proceedings of the AAAI Conference on Artificial Intelligence*, volume 39, pp. 18035–18043, 2025a.
- Lang, J., Hong, R., Cheng, Z., Zhong, T., Wang, Y., and Zhou, F. Redeeming modality information loss: Retrieval-guided conditional generation for severely modality missing learning. In *Proceedings of the 31st ACM SIGKDD Conference on Knowledge Discovery and Data Mining V. 2*, pp. 1241–1252, 2025b.
- Lee, Y.-L., Tsai, Y.-H., Chiu, W.-C., and Lee, C.-Y. Multimodal prompting with missing modalities for visual recognition. In *Proceedings of the IEEE/CVF Conference on Computer Vision and Pattern Recognition*, pp. 14943–14952, 2023.
- Li, A. C., Prabhudesai, M., Duggal, S., Brown, E., and Pathak, D. Your diffusion model is secretly a zero-shot classifier. In *Proceedings of the IEEE/CVF International Conference on Computer Vision*, pp. 2206–2217, 2023.
- Li, J., Li, D., Xiong, C., and Hoi, S. Blip: Bootstrapping language-image pre-training for unified vision-language understanding and generation. In *International conference on machine learning*, pp. 12888–12900. PMLR, 2022.
- Lin, T.-Y., Maire, M., Belongie, S., Hays, J., Perona, P., Ramanan, D., Dollár, P., and Zitnick, C. L. Microsoft coco: Common objects in context. In *European conference on computer vision*, pp. 740–755. Springer, 2014.
- Ma, M., Ren, J., Zhao, L., Tulyakov, S., Wu, C., and Peng, X. Smil: Multimodal learning with severely missing modality. In *Proceedings of the AAAI conference on artificial intelligence*, volume 35, pp. 2302–2310, 2021.

- Ma, M., Ren, J., Zhao, L., Testuggine, D., and Peng, X. Are multimodal transformers robust to missing modality? In *Proceedings of the IEEE/CVF conference on computer vision and pattern recognition*, pp. 18177–18186, 2022.
- Peebles, W. and Xie, S. Scalable diffusion models with transformers. In *Proceedings of the IEEE/CVF international conference on computer vision*, pp. 4195–4205, 2023.
- Radford, A., Kim, J. W., Hallacy, C., Ramesh, A., Goh, G., Agarwal, S., Sastry, G., Askell, A., Mishkin, P., Clark, J., et al. Learning transferable visual models from natural language supervision. In *International conference on machine learning*, pp. 8748–8763. PMLR, 2021.
- Ramesh, A., Dhariwal, P., Nichol, A., Chu, C., and Chen, M. Hierarchical text-conditional image generation with clip latents. *arXiv preprint arXiv:2204.06125*, 1(2):3, 2022.
- Rombach, R., Blattmann, A., Lorenz, D., Esser, P., and Ommer, B. High-resolution image synthesis with latent diffusion models. In *Proceedings of the IEEE/CVF conference on computer vision and pattern recognition*, pp. 10684–10695, 2022.
- Saddozai, F. K., Badri, S. K., Alghazzawi, D., Khattak, A., and Asghar, M. Z. Multimodal hate speech detection: a novel deep learning framework for multilingual text and images. *PeerJ Computer Science*, 11:e2801, 2025.
- Sharma, P., Ding, N., Goodman, S., and Soricut, R. Conceptual captions: A cleaned, hypernymed, image alt-text dataset for automatic image captioning. In *Proceedings of the 56th Annual Meeting of the Association for Computational Linguistics (Volume 1: Long Papers)*, pp. 2556–2565, 2018.
- Shi, T., Feng, W., Shang, F., Wan, L., et al. Deep correlated prompting for visual recognition with missing modalities. *Advances in Neural Information Processing Systems*, 37: 67446–67466, 2024.
- Sohl-Dickstein, J., Weiss, E., Maheswaranathan, N., and Ganguli, S. Deep unsupervised learning using nonequilibrium thermodynamics. In *International conference on machine learning*, pp. 2256–2265. pmlr, 2015.
- Wang, H., Chen, Y., Ma, C., Avery, J., Hull, L., and Carneiro, G. Multi-modal learning with missing modality via shared-specific feature modelling. In *Proceedings of the IEEE/CVF conference on computer vision and pattern recognition*, pp. 15878–15887, 2023.
- Wang, Z., Shan, X., Zhang, X., and Yang, J. N24news: A new dataset for multimodal news classification. In *Proceedings of the Language Resources and Evaluation Conference*, pp. 6768–6775, Marseille, France, June 2022. European Language Resources Association.
- Xu, H., Wu, H., Ke, X., Wu, J., Xu, R., and Xu, J. Mcmoe: Completing missing modalities with mixture of experts for incomplete multimodal action quality assessment. *arXiv preprint arXiv:2511.17397*, 2025.
- Zhang, Z., Dai, L., Lin, Q., Diao, Y., Jin, G., Guo, Y., Zhang, J., and Hao, X. Synergistic prompting for robust visual recognition with missing modalities. In *Proceedings of the IEEE/CVF International Conference on Computer Vision*, pp. 1881–1890, 2025.
- Zhao, J., Li, R., and Jin, Q. Missing modality imagination network for emotion recognition with uncertain missing modalities. In *Proceedings of the 59th Annual Meeting of the Association for Computational Linguistics and the 11th International Joint Conference on Natural Language Processing (Volume 1: Long Papers)*, pp. 2608–2618, 2021.
- Zhao, Y., Xi, W., Fu, X., and Zhao, J. Enhancing multi-modal model robustness under missing modalities via memory-driven prompt learning. In *Proceedings of the 34th International Joint Conference on Artificial Intelligence, IJCAI 2025*, pp. 2458–2466. International Joint Conferences on Artificial Intelligence, 2025.

A. Appendix

A.1. Sampling and Inference Overhead

Ablation studies on inference steps reveal that increasing the sampling steps from 50 to 500 yields negligible fluctuations in accuracy across both *N24News* and *MMHS11K* datasets; for instance, the accuracy gap in the “Both” modality of *N24News* is a mere 0.1%. This indicates that our method achieves a performance plateau at 50 DDIM steps, effectively balancing restoration quality and computational efficiency. We attribute this phenomenon to our focus on semantic-level feature restoration rather than pixel-level detail synthesis, allowing the model to satisfy the precision requirements for semantic classification with significantly fewer sampling iterations. The experimental results are shown in the Section A.1.

In comparative evaluations, while our method incurs higher latency during missing-value restoration due to the generative process, it demonstrates a pronounced speed advantage in standard inference scenarios (Both Exist), achieving a latency of only 22.94 ms with a minimal computational load of 5.02 GFLOPS. Overall, the proposed approach not only maintains superior classification accuracy under multimodal missing conditions but also ensures rapid response to complete data through a flexible inference mechanism, proving its robust adaptability and significant performance gains in practical applications.

Sample Steps	Sample Time (ms)		<i>N24News</i>			<i>MMHS11K</i>		
	Missing Text	Missing Image	Image	Text	Both	Image	Text	Both
			(70%)	(70%)	(70%)	(70%)	(70%)	(70%)
50	707.39	678.68	71.70	61.89	65.97	86.47	79.55	82.00
100	1389.02	1338.12	71.81	61.89	65.99	86.50	79.54	82.17
200	2757.05	2737.00	71.86	61.97	66.01	86.54	79.56	82.23
500	6900.35	6746.68	72.02	62.00	66.07	86.55	79.58	82.31

Table 5. Performance Stability and End-to-End Inference Efficiency across Different Sample Steps on *N24News* and *MMHS11K*.

Method	Time Cost (ms)			GFLOPS		
	Missing Text	Missing Image	Both Exist	Missing Text	Missing Image	Both Exist
MAP	202.89	374.07	550.34	90.07	135.11	180.15
MDP	43.75	41.87	41.40	41.91	41.91	41.91
DCP	25.48	28.25	23.05	16.18	16.18	16.18
SyP	25.83	27.50	23.36	16.18	16.18	16.18
RAGPT	366.61	341.85	355.07	25.65	24.72	16.66
REDEEM	379.07	348.63	362.49	27.41	26.83	17.74
Ours	707.39	678.68	22.94	112.41	82.61	5.02

Table 6. Comparison of inference efficiency and computational cost (GFLOPS) across all baseline methods under different missing modality conditions. Both inference efficiency and computational cost refer to the end-to-end metrics per single sample.

A.2. Ablation Study on Hyperparameter τ

Experimental results demonstrate that the selection of the threshold τ is pivotal in balancing the efficacy of the mutual learning mechanism with computational efficiency, as it essentially determines the timing for cross-modal alignment intervention. When τ is set excessively large (e.g., $\tau \geq 200$), the diffusion process remains in a high-noise stage where the features fed into the model contain excessive stochastic perturbations, resulting in highly ambiguous semantics for the reconstructed initial state \hat{x}_0 . In this context, the model is forced to recover semantics from nearly chaotic noise; the substantial initial feature bias prevents the mutual learning constraint from providing effective gradient guidance, ultimately leading to insignificant performance gains. Conversely, if τ is too small (e.g., $\tau < 50$), although the denoised features become more stable, the number of effective denoising steps available for calculating the mutual learning loss L_{mutual} is significantly reduced. This results in a diminished proportional contribution of the mutual learning mechanism throughout the entire inference cycle, failing to fully leverage its capability to correct semantic drift and leading to diminishing alignment returns.

Through systematic experimental observation, we found that when $\tau \in [50, 100]$, the denoising process enters a critical stage of semantic evolution, where the introduction of L_{mutual} most effectively suppresses potential semantic drifting. Compared to ablation studies using only the base loss L_{base} , performance within this interval exhibits a clearly observable and significant improvement. Notably, within the range of 50 to 100, the effectiveness of mutual learning remains relatively

stable near its peak with only minor fluctuations, demonstrating strong robustness; however, once τ falls outside this range, model performance shows a distinct downward trend. In summary, to achieve the optimal balance between the interpretability of reconstructed features, global semantic consistency, and computational cost, we propose and adopt a threshold of $\tau = 50$ for our experiments.

A.3. Integration with Other Frameworks

As a plug-and-play restorative mid-stage training module, our method offers high portability. Furthermore, since it does not alter the underlying VLM architecture, it is compatible and can be integrated with most existing missing modality approaches. The following sections analyze the broad applicability of our method and its performance when integrated with other frameworks.

To validate this scalability, we selected two representative prompt-learning frameworks, Deep Correlated Prompting (DCP) and Synergistic Prompting (SyP), as experimental baselines. Standard implementations of these methods typically resort to static learnable prompts or zero-filling strategies to compensate for missing modalities. While effective to a degree, these non-generative approaches inherently struggle to recover instance-specific semantic details. We seamlessly integrated our proposed DiT module into their inference pipelines, replacing these static placeholders with generatively restored features.

As presented in Table Section A.3, quantitative results demonstrate that augmenting existing frameworks with our method yields consistent and significant performance gains across all missing scenarios. Specifically, on the *MM-IMDb* dataset, the integrated **DCP+DiT** outperforms the original DCP by approximately **3.07%** in F1-Macro under the Image-only condition (rising from 51.15% to 54.22%), and by **2.38%** under the Text-only condition. Similar trends are observed with **SyP+DiT** on the *N24News* dataset, where the module boosts accuracy by **3.73%** (from 67.73% to 71.46%) in the Image-only scenario. These results strongly support our claim that the proposed module serves as a universal, performance-enhancing plugin that effectively bridges the semantic gap in existing systems without compromising their original architectural integrity.

Method	MM-IMDb			N24News			MMHS11K		
	Image (70%)	Text (70%)	Both (70%)	Image (70%)	Text (70%)	Both (70%)	Image (70%)	Text (70%)	Both (70%)
DCP	51.15	47.58	47.47	67.82	57.83	61.82	71.66	73.64	70.38
DCP + DiT	54.22	49.96	48.10	71.56	58.17	62.64	75.61	74.22	71.31
SyP	50.16	46.52	48.02	67.73	57.64	61.73	70.73	73.87	70.85
SyP + DiT	52.92	46.89	48.65	71.46	59.07	62.55	72.61	75.45	71.79

Table 7. Performance comparison validating the effectiveness of integrating our DiT module with DCP and SyP baselines. Experiments are conducted on three downstream datasets *MM-IMDb*, *N24News*, *MMHS11K*) with a missing ratio of 70%. "Image", "Text", and "Both" denote the specific available modality conditions. Results demonstrate that the integration of our DiT module consistently improves performance across all settings compared to the original baselines.

A.4. Additional Analysis across Various Missing Rates.

As shown in Figure 8, We conducted additional experiments in all missing modality scenarios including image missing.

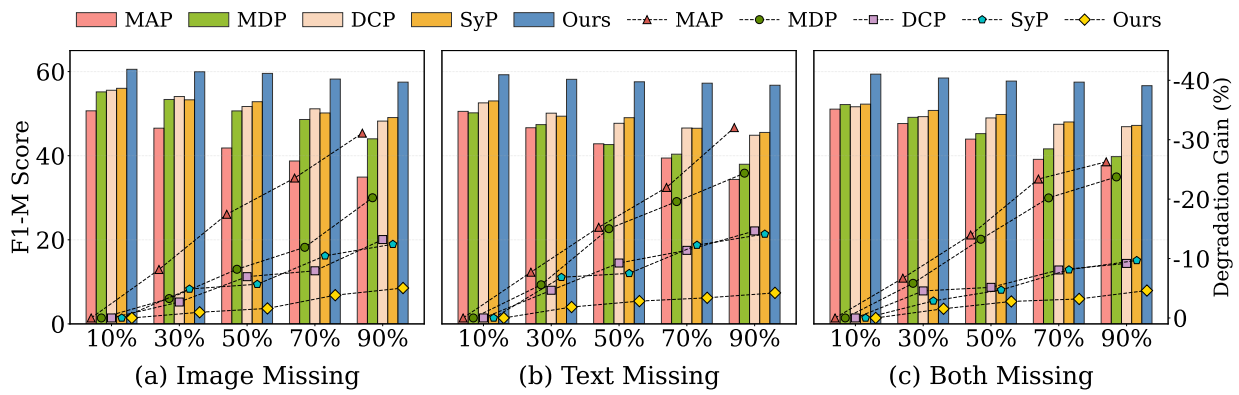


Figure 8. Robustness analysis (missing image, missing text and both missing) on the *MM-IMDb* dataset across various missing rates.